growth results in a porous outer layer (*15*). Other researchers have correlated the transition in polymer morphology with a decrease in the polymer conductivity (*20*), although an unambiguous mechanism for the transition has not yet been proposed. However, the similarity between the polymer morphologies of fibers and thin films suggests that the uniformity of the fibers and the high current efficiency result from a decrease in the polymer conductivity in the outer porous layer of the fiber, allowing essentially all of the current to flow to the tip.

The effect of the cell geometry in governing the direction of the fiber growth, demonstrated in Fig. 2, is undoubtedly related to hydrodynamic flow patterns at the tip. The flow of the electrolyte past the fiber tip results in a relatively stagnant fluid layer for which the residence time of chemical intermediates is significantly longer than at the side surface of the fiber. We demonstrated this by inserting a Pt cylindrical electrode 127 μm in diameter in the capillary cell, oriented with its axis perpendicular to the direction of flow. When an anodic current was applied, poly(3-MT) deposition occurred noticeably faster on the back side of the cylindrical electrode than elsewhere, consistent with our hypothesis that the polymer deposition is highest in regions where the residence time of the intermediates is largest. Given this experimental observation, a change in flow direction produced by the cell geometry would tend to orient the direction of the fiber growth in the direction of the flow, consistent with our experimental results. Our results are also consistent with the results of a rotating disk electrode experiment (*21*), in which a polypyrrole film was deposited preferentially at the center of the rotating disk where the fluid velocity is the smallest.

REFERENCES AND NOTES

1. D. Jeon, J. Kim, M. C. Gallagher, R. F. Willis, *Science* **256**, 1662 (1992); J. Heinze, *Top. Curr. Chem.* **152**, 1 (1990); N. C. Billingham and P. D. Calvert, *Adv. Polym. Sci.* **90**, 1 (1989).
2. A. J. Heeger *et al.*, *Synth. Metals* **41–43**, 1027 (1991).
3. J. H. Burroughs *et al.*, *Nature* **347**, 539 (1990); A. J. Heeger *et al.*, *ibid.* **357**, 539 (1992); P. L. Burn *et al.*, *ibid.* **356**, 47 (1992).
4. H. S. White, G. P. Kittlesen, M. S. Wrighton, *J. Am. Chem. Soc.* **106**, 5375 (1984); G. P. Kittlesen, H. S. White, M. S. Wrighton, *ibid.*, p. 7389; D. Bloor, *Nature* **349**, 738 (1991).
5. R. Bittihn *et al.*, *Makromol. Chem. Macromol. Symp.* **8**, 52 (1987); R. J. Mammone and M. Binder, *J. Electrochem. Soc.* **135**, 1057 (1988).
6. C. B. Duke, *Synth. Metals* **21**, 5 (1987); S. Roth, *ibid.*, p. 51; A. G. MacDiarmid, *ibid.*, p. 79.
7. Z. Deng, W. H. Smyrl, H. S. White, *J. Electrochem. Soc.* **136**. 2152 (1989).
8. D. D. C. Bradley *et al.*, *Synth. Metals* **17**, 473 (1987); J. M. Machado, M. A. Masse, F. E. Karasz, *Polymer* **30**, 1992 (1989).
9. P. Smith *et al.*, *Polymer* **33**, 1102 (1992); M. Ponerantz *et al.*, *Synth. Metals* **41–43**, 825 (1991).
10. A. Andreatta, Y. Cao, J. C. Chiang, A. J. Heeger, P. Smith, *Bull. Am. Phys. Soc.* **34**, 582 (1989); X. Tang, E. Scherr, A. G. MacDiarmid, A. J. Epstein, *ibid.*, p. 583.
11. J. R. Reynolds, M. B. Gieselman, Y.-J. Qiu, M. H. Pyo, *Polym. Mater. Sci. Eng.* **64**, 202 (1991); W. Wernet, *Synth. Metals* **41–43**, 843 (1991); N. Bates, M. Cross, R. Lines, D. Walton, *J. Chem. Soc. Chem. Commun.* **1985**, 871 (1985); L. P. Rector, D. C. De Groot, J. L. Marks, S. H. Carr, *Synth. Metals* **41–43**, 935 (1991).
12. C. R. Martin, Z. Cai, L. S. Van Dyke, W. Liang, *Polym. Mater. Sci. Eng.* **64**, 204 (1991).
13. 3-Methylthiophene (Aldrich) was distilled under ambient pressure. Tetrabutylammonium perchlorate (Kodak) was recrystallized twice in ethyl acetate and dried in vacuum. Acetonitrile (Aldrich) was used as received.
14. A Pine Instrument RDE4 potentiostat-galvanostat was used to supply a constant current to the electrochemical flow cell. The JEOL 840II scanning electron microscope was used to examine the fiber. X-ray diffraction patterns were obtained on a CAD-4 diffractometer.
15. G. Tourillon and F. Garnier, *J. Phys. Chem.* **87**, 2289 (1987).
16. S. Li and H. S. White, in preparation.
17. G. Tourillon and F. Garnier, *J. Polym. Sci. Polym. Phys. Ed.* **22**, 33 (1988).
18. Reynold's number is calculated: $Re = V_{ave}d_e/\gamma$, where V_{ave} is the average flow velocity (in centimeters per second), d_e is the difference (in centimeters) in the diameters of the cell glass tube and the Pt electrode, and γ is the kinematic viscosity of acetonitrile, 4.23×10^{-3} cm^2 s^{-1}.
19. E. M. Genies, G. Bidan, A. F. Diaz, *J. Electroanal. Chem.* **149**, 101 (1983).
20. T. F. Otero and E. L. Azelain, *Polymer* **29**, 1522 (1988).
21. P. Lang, F. Chao, M. Costa, F. Garnier, *ibid.* **28**, 668 (1987).

22. This work was supported by the Office of Naval Research and the Center for Interfacial Engineering (NSF Engineering Research Centers Program). We thank D. Britton (University of Minnesota) for the x-ray diffraction analysis.

29 September 1992; accepted 18 December 1992

Colicin E1 Binding to Membranes: Time-Resolved Studies of Spin-Labeled Mutants

Yeon-Kyun Shin, Cyrus Levinthal, Françoise Levinthal, Wayne L. Hubbell*

To investigate the mechanism of interaction of the toxin colicin E1 with membranes, three cysteine substitution mutants and the wild type of the channel-forming fragment were spin labeled at the unique thiol. Time-resolved interaction of these labeled proteins with phospholipid vesicles was investigated with stopped-flow electron paramagnetic resonance spectroscopy. The fragment interacts with neutral bilayers at low pH, indicating that the interaction is hydrophobic rather than electrostatic. The interaction occurs in at least two distinct steps: (i) rapid adsorption to the surface; and (ii) slow, rate-limiting insertion of the hydrophobic central helices into the membrane interior.

Colicins are water-soluble cytotoxins secreted by and active against *Escherichia coli* (*1*). The secreted toxin binds to a receptor in the bacterial outer membrane and is transported into the periplasmic space, where it inserts into the inner membrane to form voltage-sensitive ion channels. Structural domains (receptor binding, translocation, and channel formation) of the protein subserve distinct steps of the cytotoxic process. The functional channel-forming domain of colicin E1, consisting of an ~20-kD COOH-terminal fragment, is readily isolated by trypsinolysis (*2*). The crystal structure of the analogous fragment of colicin A was recently solved (*3*, *4*); the core of the molecule consists of two extremely hydrophobic α helices and is surrounded by eight amphipathic α helices. Two-dimensional nuclear magnetic resonance (NMR) studies (*5*) generally support a similar structure for the corresponding colicin E1 fragment. With this information, a structural model of colicin E1 was generated (Fig. 1A) (*6*).

The channel-forming fragments of colicin A and E1 interact irreversibly with membranes at acidic pH. Although the structure of the membrane-bound form is unknown, the helical content is similar to the soluble form (*7*), and there is evidence for the insertion of the two core helices into the membrane interior (Fig. 1B) (*8*). In many ways, the colicin channel-forming fragment is similar to the translocation domain of diphtheria toxin, which consists of nine α helices, two of which are hydrophobic (*9*). Membrane insertion and channel formation of diphtheria toxin are triggered by acidic pH. Thus, studies of the colicins may also be germane to the mechanism of action of other toxins.

The recently introduced method of site-directed spin labeling (SDSL) is well suited to time-resolved analysis of structural changes in proteins. In this method, cysteine substitution mutants are used to provide specific attachment sites for nitroxide spin labels. Electron paramagnetic reso-

Y.-K. Shin and W. L. Hubbell, Jules Stein Eye Institute and Department of Chemistry and Biochemistry, University of California, Los Angeles, CA 90024.
C. Levinthal and F. Levinthal, Department of Biological Sciences, Columbia University, New York, NY 10027.

*To whom correspondence should be addressed.

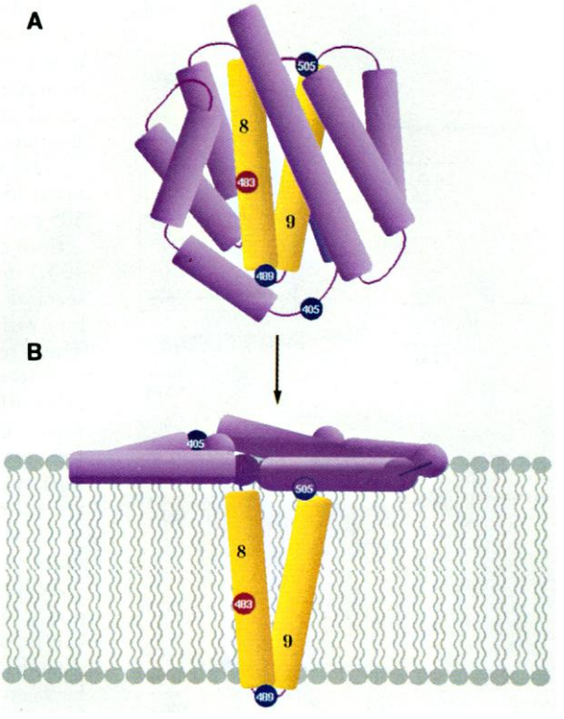

Fig. 1. Structural model for the colicin E1 channel-forming fragment. (**A**) Hydrophobic central helices are numbered 8 and 9, and the spin-labeled sites are indicated by their colicin E1 sequence numbers. The exact location of the labeled sites is not critical for the present purposes, and only the general topological location is implied. (**B**) Proposed structure for the colicin E1 fragment in the membrane-bound state.

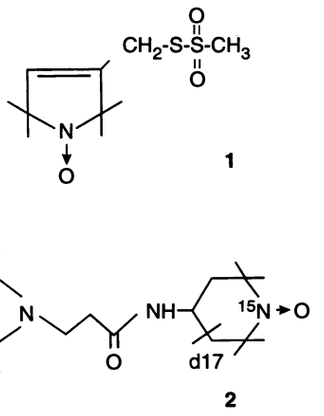

Fig. 3. Nitroxide spin labels.

nance (EPR) analysis of such spin-labeled proteins has yielded information on the topology and secondary structure of the polypeptide chain as well as on tertiary interactions of the labeled site (*10–12*). In the present work we combine SDSL with rapid-mixing EPR spectroscopy (*13*) to investigate the molecular details of colicin-membrane interactions.

A mechanism for the insertion of colicin into membranes is proposed in Fig. 2 (*3*, *14*). The distinguishable steps are as follows: (i) protonation of the colicin molecule to produce an active state; (ii) diffusion to the membrane surface phase; (iii) adsorption of the proper orientation to the membrane surface; and (iv) insertion into the membrane. There is much experimental support for the first protonation step, and early studies suggested that protonation may produce a molten globule state in toxins at acidic pH (*15–17*). The third step leads to an adsorbed state that precedes insertion. Although the presence of a transient adsorbed state has been inferred from kinetic data (*14*), direct evidence for its existence is lacking. The objective of the present study is to provide definitive evidence for the existence of an adsorbed state preceding the inserted form and to provide new evidence consistent with the structure of the membrane-bound state (Fig. 1).

A nitroxide side chain located in the hydrophobic helix 8 would serve as an ideal probe to resolve the final insertion event because helix 8 is buried within the protein interior and the nitroxide is allowed little motion relative to the protein (Fig. 1A) in solution. In the inserted state, on the other hand, the nitroxide would face the fluid hydrocarbon chains of the bilayer and have rapid motion relative to the protein (Fig. 1B).

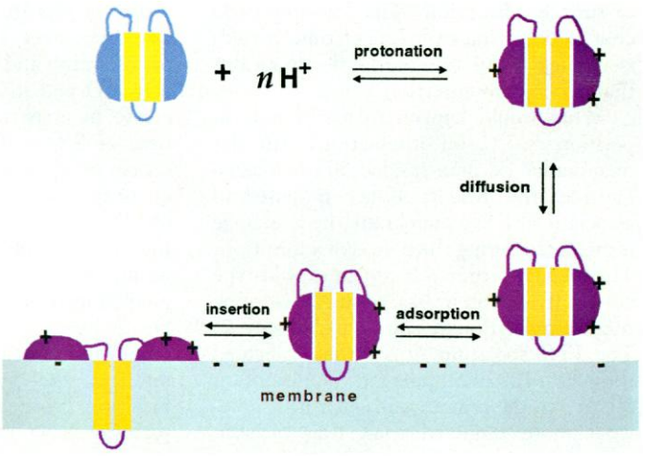

Fig. 2. Proposed mechanism for insertion of colicin E1 into membranes. The colicin COOH-terminal fragment is schematically represented for simplicity.

To test these ideas, we prepared the COOH-terminal fragment of the colicin E1 mutant L483C (*18*) and reacted it with the sulfhydryl-selective methanethiosulfonate spin label **1** (Fig. 3) (*10*, *11*, *19*). The EPR spectrum of this mutant in solution indicated that the nitroxide was immobilized; the rotational correlation time estimated by lineshape simulation (*20*) was ~10 ns, close to the value expected for that of the 20-kD fragment in water.

After mixing with vesicles of dilauroylphosphatidylcholine (DLPC), there was an increase in the mobility of the side chain at equilibrium (Fig. 4A). Several features of the EPR spectra indicated that the nitroxide faced the fluid hydrocarbon chains of the bilayer in this bound state. First, the solvent-sensitive hyperfine coupling constant corresponded to a relatively nonpolar environment and was similar to that for nitroxides on the external surface of a transmembrane helix in bacteriorhodopsin (*10*). Second, the nitroxide was inaccessible to collision with chromium oxalate in the aqueous phase, whereas the collision rate with the hydrophobic radical O_2 was high. These results are indicative of nitroxides in the bilayer interior (*10*) and strongly support insertion of helix 8. They also indicate that colicin E1 binds not only to negatively charged membranes but also to neutral membranes. The insertion event revealed by spin-labeled L483C (Fig. 4A) was a first-order process with a half-time of 127 ± 4 s.

Does an adsorbed state precede the insertion, or are these events concerted? The major change on adsorption is postulated to be a simple reduction in rotational diffusion of the protein. Hence, the lineshape of the nitroxide at residue 483, already in a slow

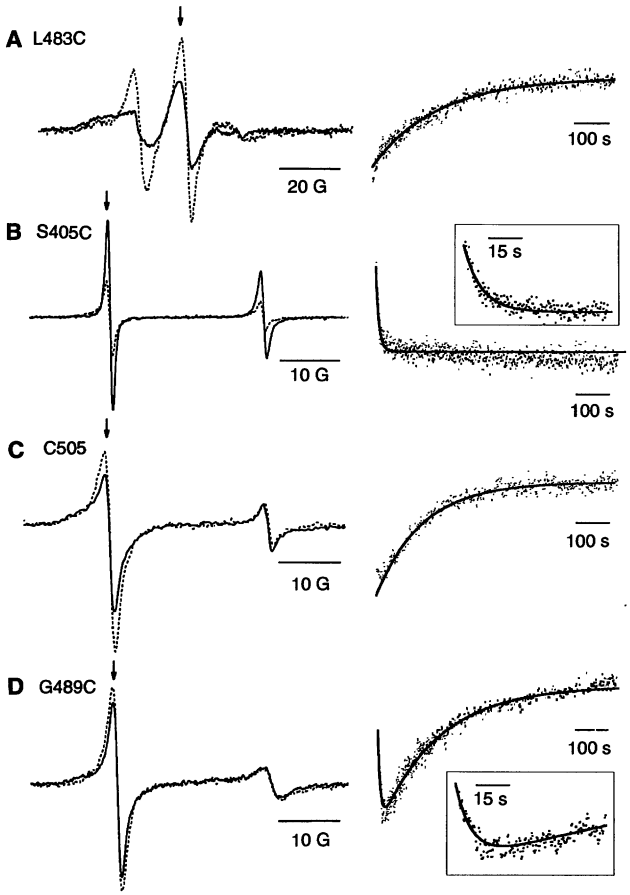

Fig. 4. Equilibrium and time-resolved changes in EPR spectra of spin-labeled colicin mutants. (**A**) Spin label **1** on L483C; (**B**) spin label **2** on S405C; (**C**) spin label **2** on C505; and (**D**) spin label **2** on G489C. Each part shows a pair of spectra for the indicated spin-labeled mutant. The solid line corresponds to the solution spectrum of the labeled fragment in 50 mM formic acid–NaOH buffer, pH 2.7, and the dotted line corresponds to the labeled fragment bound to extruded (*25*) DLPC vesicles (50-nm diameter) in the same buffer. More than 95% of the fragment is in the bound form. After rapid mixing of the protein and vesicles, each in the above buffer, the spectral intensity as a function of time was recorded at the position indicated by the arrow and shown to the right of each pair of spectra. The protein concentration after mixing was ~15 μM, and the final lipid:protein molar ratio was 2000:1. The solid lines on the time recordings are least-squares fits to single first-order processes. In (D), the fit is to two consecutive first-order processes.

motional regime, would not be very sensitive to further reduction in motion and would not detect adsorption. On the other hand, an adsorbed state (Fig. 2) could be detected by a nitroxide at a position such as 405, in a solvent-exposed loop. A nitroxide at this position would undergo rapid motion when the fragment is free in solution. If membrane association occurs in the proposed orientation (Fig. 2), the nitroxide would then be located in the viscous head-group region of the bilayer and experience reduced mobility. What would happen upon subsequent insertion? If the proposed model is correct, little change is expected because the interhelical loop containing residue 405 would remain in the head-group region (Fig. 1B).

To test these predictions, we prepared the tryptic fragment of mutant S405C and labeled it with the ^{15}N-containing nitroxide maleimide **2** (Fig. 3) (*21*), which was designed with a spacer arm between the attachment point and the nitroxide to allow rapid motion relative to the protein. The size of this label was not expected to perturb the structure of the protein because the label was at a surface site (*22*). The EPR spectrum of the water-soluble fragment had narrow resonance lines, indicating rapid motion of the side chain relative to the fragment (Fig. 4B). In the membrane-bound form, the spectral amplitude was significantly attenuated, indicating reduced motion, which is consistent with the adsorption model. The time course of the decay in amplitude was a first-order process (Fig. 4B) with a half-time of 6.2 ± 0.4 s, which is much faster than that observed for the 483 mutant. Thus, upon interaction with vesicles, the nitroxide at residue 405 detects a process that precedes insertion and that is consistent with the expectations of surface adsorption. The low-amplitude change occurring over longer time periods is apparently due to more subtle alterations that accompany insertion.

What would happen to a nitroxide at position 505 upon interaction with the membrane? Because residue 505 is located far from the protein surface proposed to associate with the membrane, little change is predicted during the period of adsorption. The COOH-terminal fragment of wild-type colicin E1, which has a single cysteine residue at position 505, was labeled with **2**. The EPR spectrum in solution indicated that the nitroxide undergoes rapid motion relative to the protein, although it is somewhat more hindered than that of 405. Nevertheless, a high collision rate with chromium oxalate in solution indicated that a nitroxide at this position is exposed to water (*11*). In the inserted state, the signal amplitude of the spectrum became sharper and was similar to that of 405.

The time course of the spectral change revealed that the surface on which residue 505 resides does not show significant interactions on the time scale of adsorption (Fig. 4C). Instead, there was an increase of spectral amplitude on a time scale consistent with insertion (half-time at 95 ± 4 s). These results strongly suggest that adsorption is vectorial and that it occurs in the orientation indicated (Fig. 2). That changes are detected at residue 505 upon insertion is expected because disruption of the tertiary fold would relieve steric constraints around residue 505.

Considering that the 405 and 483 mutants resolve events of a very different time scale, probably corresponding to adsorption and insertion, respectively, an experiment can be designed to test this interpretation. A spin label at residue 489, in the loop between helices 8 and 9 (Fig. 1A), should be in rapid motion relative to the protein in solution because the side chain is in a solvent-exposed loop. Upon adsorption to the membrane surface, the nitroxide should experience a reduction in motion because it is exposed on the surface of the fragment proposed to interact with the bilayer (the same surface as 405). This reduction in motion should be reversed upon insertion, provided that the loop between helices 8 and 9 is again solvent exposed as proposed (Fig. 1B). Thus, two sequential events should be observed: a reduction in motion with the time course of adsorption and an increase in motion with the time course of insertion. The final and initial spectra should be similar.

To test this postulate, we spin labeled the tryptic fragment of G489C with **2**. There was little difference between the EPR spectra in solution and after insertion (Fig. 4D), and the hyperfine coupling indicates that the nitroxide was in the water phase in both cases. However, the separate kinetic events of adsorption and insertion are well resolved (Fig. 4D and inset). The initial rapid decrease in amplitude occurred with a half-time of 5.5 ± 0.4 s, similar to the time course of adsorption (Fig. 4B). The subsequent increase in amplitude has a half-time of 121 ± 2.4 s, close to that for insertion, as the signal returns to its original state. These results are in complete accord with the predictions of the mechanism presented in Fig. 2.

Several conclusions can be drawn as a result of the present study. (i) Colicin insertion proceeds along the mechanistic pathway shown in Fig. 2, with an oriented,

adsorbed state as an intermediate and with insertion as the rate-limiting step. The ability to resolve adsorption from insertion will permit investigation of the effects of pH, ionic strength, surface potential, and lipid compositions on these events independently. (ii) Colicin E1 adsorbs to and inserts into neutral membranes at acidic pH, and the basis of the interaction is thus likely hydrophobic. (iii) The absence of spectral change at residues 483 and 505 during adsorption suggests that the structure of the adsorbed state is similar to that in solution. (iv) The data presented are consistent with the insertion of helix 8 into the bilayer interior and the complete passage of the 8-9 interhelical loop across the membrane, although they cannot eliminate another recently proposed model in which the 8-9 interhelical loop remains in the solution on the same side to which the colicin was added (*23*).

Although the rates of the processes investigated here are slow, rapid-mixing EPR instrumentation presently available permits investigation of processes on the order of milliseconds (*13*, *24*). Thus, site-directed spin-labeling methods of the type illustrated here can be used to investigate other, more rapid time-dependent molecular events such as protein folding.

REFERENCES AND NOTES

1. W. A. Cramer, F. S. Cohen, A. R. Merrill, H. Y. Song, *Mol. Microbiol.* **4**, 519 (1990); C. J. Lazdunski *et al.*, *Biochim. Biophys. Acta* **947**, 445 (1988).
2. J. O. Bullock, F. S. Cohen, J. R. Dankert, W. A. Cramer, *J. Biol. Chem.* **258**, 9908 (1983).
3. M. W. Parker, F. Pattus, A. D. Tucker, D. Tsernoglou, *Nature* **337**, 93 (1989).
4. M. W. Parker, J. P. Postma, F. Pattus, A. D. Tucker, D. Tsernoglou, *J. Mol. Biol.* **224**, 639 (1992).
5. M. R. Wormald, A. R. Merrill, W. A. Cramer, R. J. P. Williams, *Eur. J. Biochem.* **191**, 155 (1990).
6. The structural model for colicin E1 was constructed by L. Salwinski with HOMOLOGY software (Biosym Technologies, San Diego, CA).
7. P. Rath, O. Bousche, A. R. Merrill, W. A. Cramer, K. J. Rothschild, *Biophys. J.* **59**, 516 (1991); E. Goormaghtigh *et al.*, *Eur. J. Biochem.* **202**, 1299 (1991).
8. J. H. Lakey *et al.*, *Eur. J. Biochem.* **196**, 559 (1991); J. H. Lakey, D. Baty, F. Pattus, *J. Mol. Biol.* **218**, 639 (1991); H. Y. Song, F. S. Cohen, W. A. Cramer, *J. Bacteriol.* **173**, 2927 (1991); C. K. Abrams, K. S. Jakes, A. Finkelstein, S. L. Slatin, *J. Gen. Physiol.* **98**, 77 (1991); M. vB. Cleveland, S. L. Slatin, A. Finkelstein, C. Levinthal, *Proc. Natl. Acad. Sci. U.S.A.* **80**, 3706 (1983).
9. S. Choe *et al.*, *Nature* **357**, 216 (1992).
10. C. Altenbach, T. Marti, H. G. Khorana, W. L. Hubbell, *Science* **248**, 1088 (1990).
11. A. P. Todd, J. Cong, F. Levinthal, C Levinthal, W. L. Hubbell, *Proteins* **6**, 294 (1989).
12. D. A. Greenhalgh, C. Altenbach, W. L. Hubbell, H. G. Khorana, *Proc. Natl. Acad. Sci. U.S.A.* **88**, 8626 (1991).
13. W. L. Hubbell, W. Froncisz, J. S. Hyde, *Rev Sci. Instrum.* **58**, 1879 (1987).
14. J. M. Gonzalez-Manas, J. H. Lakey, F. Pattus, *Biochemistry* **31**, 7294 (1992).
15. O. B. Ptitsyn, *J. Protein Chem.* **6**, 273 (1987).
16. F. G. van der Goot, J. M. Gonzalez-Manas, J. H. Lakey, F. Pattus, *Nature* **354**, 408 (1991).
17. A. R. Merrill, F. S. Cohen, W. A. Cramer, *Biochemistry* **29**, 5829 (1990).
18. The preparation of cysteine substitution mutants of colicin E1 with the single wild-type cysteine replaced by glycine has been described previously [Q. R. Liu *et al.*, *Proteins* **1**, 218 (1986)]. All spin-labeled mutants investigated have wild-type killing activity against sensitive strains.
19. L. J. Berliner, J. Grunwald, H. O. Hankovszky, K. Hideg, *Anal. Biochem.* **119**, 450 (1982).
20. E. Meirovitch, A. Nayeem, J. H. Freed, *J. Phys. Chem.* **88**, 3454 (1984).
21. G. Wu, thesis, University of California, Los Angeles (1992). Nearly complete labeling of Cys^{405} and Cys^{489} with **2** was attained within 3 to 4 hours at 20°C, pH 7.2, with a 1 to 4 ratio of protein to spin label. Spin label **2** was synthesized by G. Wu.
22. J. U. Bowie, J. F. Reidhaar-Olson, W. A. Lim, R. T. Saur, *Science* **247**, 1306 (1990).
23. J. H. Lakey, J. M. Gonzalez-Manas, F. G. Vandergoot, F. Pattus, *FEBS Lett.* **307**, 26 (1992).
24. J. J. Jiang, J. F. Bank, W. W. Zhao, C. P. Scholes, *Biochemistry* **31**, 1331 (1992).
25. Y.-K. Shin and W. L. Hubbell, *Biophys. J.* **61**, 1443 (1992).

26. We thank C. Altenbach for assistance with figures; M. Parker for supplying the colicin A coordinates; and J.-P. Cong and L. Manzano for assistance with colicin mutant development and production, respectively. Supported by NIH grant EY05216, a grant from Research to Prevent Blindness, and the Jules Stein Professor endowment.

27. This work is dedicated to the memory of Professor Cyrus Levinthal.

23 September 1992; accepted 25 November 1992

The Secretory Granule Matrix: A Fast-Acting Smart Polymer

Chaya Nanavati* and Julio M. Fernandez†

The secretory granule matrix is a miniature biopolymer that consists of a charged polymer network that traps peptides and transmitters when it condenses and releases them on exocytotic decondensation. Models of exocytotic fusion have treated this matrix as a short circuit and have neglected its electrical contributions. This matrix responded to negative voltages by swelling, which was accompanied by a large increase in conductance, and to positive voltages by condensing. Thus, the matrix resembled a diode. The swollen matrix exerted large pressures on the order of 12 bar. The responses took place within milliseconds of the application of the electric field. These findings suggest that matrix decondensation, and therefore product release, is controlled by potential gradients.

Most granule matrices are too small to be studied, but the relatively large (5-μm-diameter) matrices in the secretory granule of the mast cells of the beige (bg^J/bg^J) mouse are an exception. They contain a negatively charged heparin sulfate proteoglycan network that condenses in the presence of divalent cations, such as calcium or histamine (at acid pH), and decondenses in the presence of monovalent cations, such as sodium (*1*, *2*). We studied the electrical properties of the secretory granule matrices of beige mice by placing the matrices in the tip of a glass pipette (*3*).

Several properties of the granule matrix changed dramatically in response to a change in the applied voltage. At zero or positive pipette potentials, the granule matrix was refractile and condensed and conducted poorly (Fig. 1, A and B). In contrast, at negative potentials, the matrix was transparent and swollen and conducted a large inward current. The matrix had swollen to half of its final size within one video frame of the application of a potential of −2.5 V. The instantaneous swelling was followed by a slower exponential phase (Fig. 1B) (*4*). At the same time, we observed an instantaneous (≤2.5 ms) inward current, which was half of the final value. As with the swelling, this instantaneous current was followed by a slower exponential phase (Fig. 1B) (*4*). When the voltage was turned off, both the current and the swelling returned to control levels within 300 ms. If we assume that the voltage dropped across the diameter of the matrix, the 2.5 V across the 5-μm matrix equaled a field strength of 5000 V cm^{-1}. For comparison, the 50-mV transmembrane potential that is necessary to open a sodium channel corresponds to an electric field of 50,000 V cm^{-1}. Therefore, the electric field needed to trigger matrix swelling is smaller than that required to open an ion channel.

In exocytosis, the secretory granule matrix expands against the cellular cytoskeleton (*5*). To see if a granule matrix subjected to an electric field could perform mechanical work, we used a miniature stress transducer to measure the force exerted by a swollen matrix (Fig. 1C) (*6*). We obtained a value of 131 ± 38 μg (mean ± SD; n = 5) (*7*); if 1 μm^2 of the granule is in contact with the stress transducer, this force translates to a pressure of ~12 bar.

Both the magnitude of the current through the matrix and the amount of swelling depended on voltage and displayed

Department of Physiology and Biophysics, Mayo Clinic, MSB 1-117, Rochester, MN 55905.

*Present address: Department of Cell Biology, Duke University Medical Center, Durham, NC 27710.
†To whom correspondence should be addressed.